JOURNAL OF GEOPHYSICAL RESEARCH, VOL. 101, NO. C1, PAGES 923–939, JANUARY 15, 1996

Intensive surveys of the Azores Front
1. Tracers and dynamics

Daniel L. Rudnick
Scripps Institution of Oceanography, La Jolla, California

James R. Luyten
Woods Hole Oceanographic Institution, Woods Hole, Massachusetts

Abstract. The hypothesis that fronts are sites of active subduction is examined using density, temperature, salinity, and horizontal velocity data from a trio of surveys of the Azores Front done in May 1991 and March 1992. These surveys were made using a SeaSoar equipped with a conductivity-temperature-depth profiler and a shipboard acoustic Doppler current profiler. The potential density and potential vorticity indicate that dense water from the north side of the front may be sliding down beneath the surface outcrop. This apparently subducting isopycnal has a great deal of temperature and salinity variability. Horizontal velocity is nearly parallel to isopycnals, indicating that the time rate of change and vertical advection must be small. The thermal wind balance is observed to be valid, especially in the region of the largest horizontal density gradients. Shear at the base of the mixed layer is likely due to near-inertial motions. The potential vorticity is dominated by the planetary vorticity, except at the front, where vertical shears (the tilting term) become large. The tilting term acts to reduce the magnitude of the potential vorticity at the front, in agreement with simple theoretical models. The magnitude of the tilting term is similar to the total vorticity in the seasonal thermocline.

1. Introduction

The similarity in properties of water masses in the upper thermocline to late winter surface waters has been well established. *Iselin* [1939] first noted the similarity in the temperature-salinity (T-S) curves for north-south surface sections and vertical profiles in the subtropical gyre. He further suggested the possibility that March surface water moves along isopycnals to set the T-S relationship in the thermocline. *Stommel* [1979] proposed a mechanism (the so-called Ekman demon) by which water from the base of the year's deepest mixed layer in March is then swept into the interior by Ekman pumping in a region of Sverdrup dynamics. A relatively simple model of this process, neglecting mixed-layer dynamics, was presented by *Luyten et al.* [1983]. The rate of this process, sometimes called subduction, is set by the Ekman pumping vertical velocity at order 10^{-6} m s^{-1} [*Isemer and Hasse*, 1987].

What is the mechanism by which the water escapes the mixed layer? Using the concept of an entrainment velocity [*de Szoeke*, 1980], *Nurser and Marshall* [1991] assumed continuity across the mixed-layer base and determined the "subduction velocity" (the negative of the entrainment velocity) to be proportional to the net heat flux. The apparent result is that subduction is possible only in the presence of net surface heating. It is reasonable to ask if subduction might be possible in the absence of any heating.

The hypothesis of this study is that oceanic fronts are sites of active subduction. Two essential characteristics of fronts lead to this hypothesis. First, fronts are often sites of surface convergence which may, to some extent, be balanced by localized downwelling. Second, because of large horizontal density gradients, fronts are regions of enhanced vertical shear and possibly strong vertical mixing. The thrust here is to present evidence of the first characteristic. While it will be shown that shear is increased at fronts, no direct observations of mixing are presented. We investigate subduction at fronts through an intensive description of a series of fronts and a careful examination of frontal dynamics.

The importance of vertical circulation at fronts has been demonstrated by a number of studies. *Pollard and Regier* [1990, 1992] have examined vertical circulation through tracers and by the solution of the omega equation. These studies of the subtropical front in the western North Atlantic have inferred vertical velocities as strong as 40 m d^{-1}. *Rudnick and Weller* [1993] have calculated the vertical velocity necessary to close the heat budget using a moored array of current meters and have found similar magnitudes. The goal of this paper is to demonstrate the likelihood of strong vertical velocities by examining tracer fields. The quantification of vertical velocity will be addressed in part 2 [*Rudnick*, 1996].

We investigate the hypothesis that fronts are sites of subduction with a trio of surveys of the Azores Front, one in May 1991 and two in March 1992. The surveys were conducted using a SeaSoar equipped with a conductivity-temperature-depth (CTD) profiler and a shipboard acoustic Doppler current profiler (ADCP). A summary of the surveys and data is given in section 2. Results are presented in vertical sections across the front and horizontal maps; the mapping procedure is described in section 3. The hydrographic variables are presented in section 4. The velocity, dynamics, and potential vorticity are discussed in section 5. Finally, section 6 provides a summary and conclusions.

Paper number 95JC02867.
0148-0227/96/95JC-02867$05.00

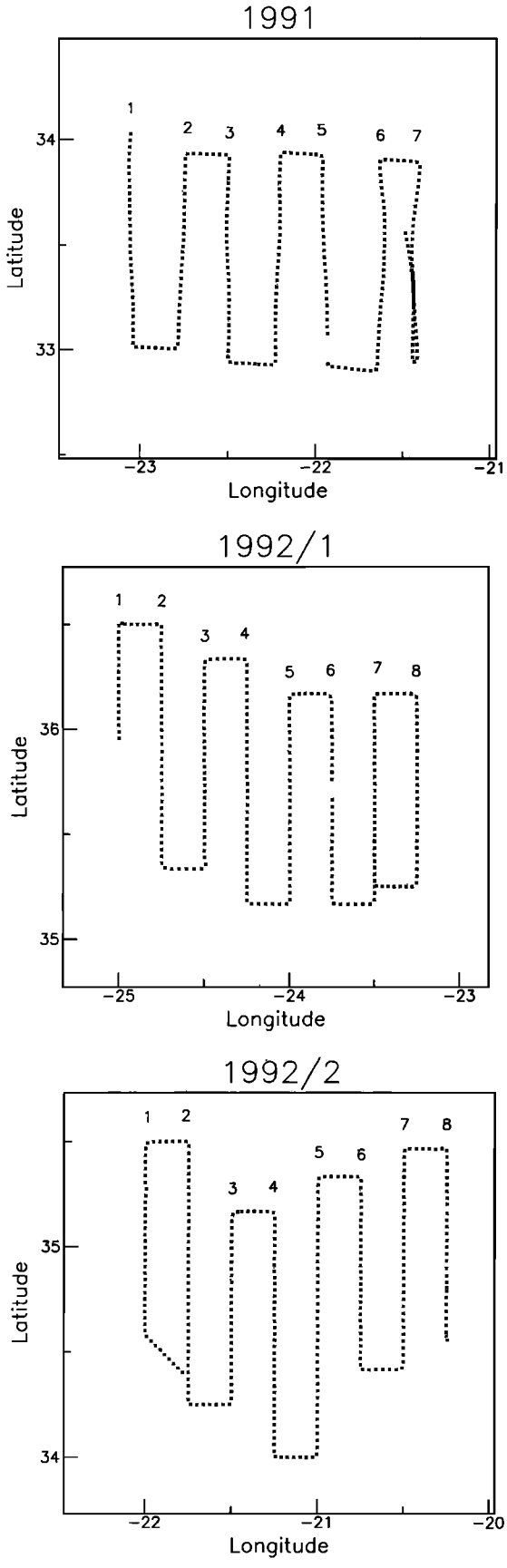

Figure 1. Locations of SeaSoar bins for the three surveys. The bins are 15 min in time by 8 m in the vertical. Leg numbers are indicated. Short gaps are caused by failures in data acquisition.

2. Data

The objective of the experiment was to make high-resolution surveys of the Azores Front. The first problem was then to locate the front quickly and accurately. The search was aided using satellite sea surface temperature (SST) images brought to the ship from shore using Inmarsat. While steaming at full speed (with the SeaSoar on deck), observations of SST and current were monitored. The front was readily indicated by a rapid change of SST and, especially, a strong eastward current. Upon finding a section of front, the SeaSoar was deployed.

The SeaSoar carried a Sea-Bird CTD equipped with two conductivity sensors, two thermistors, an oxygen sensor, and a fluorometer. The conductivity sensors were mounted on the top of the vehicle as far forward as possible and oriented into the flow. The thermistors were just aft of the conductivity sensors and angled up to encounter undisturbed flow. The calibration of these sensors is discussed in the appendix; oxygen and fluorescence data are not presented here.

The surveys consisted of a series of N-S sections of roughly a degree in latitude across the nearly E-W trending front, with a spacing between sections of about 1/4° of longitude. At a towing speed of approximately 4 m s^{-1} the SeaSoar completed four to six cycles per hour from the surface to 350 m or deeper, while the ADCP collected 5-min ensembles. These data were averaged into bins of 15 min in time (a horizontal resolution of about 3.5 km) by 8 m in depth (Figure 1). The length of the bins ensured that the SeaSoar completed at least one cycle per bin, while the depth was set by the resolution of the ADCP. The coverage in depth was fairly consistent, although there were times when the SeaSoar had shallow dives.

The challenge in the initial analysis is the merging of three distinct data sets: Global Positioning System (GPS) navigation, CTD, and ADCP. Each of these data must be processed with special attention to the different characteristics of the instrumentation. Pertinent details of the processing are presented in the appendix.

3. Maps

Many of the results of these surveys are presented in the form of vertical sections or horizontal maps. The goal of the vertical sections of directly observed quantities is to obtain the highest-resolution picture possible. Because the resolution in the E-W and N-S directions is very different, careful attention must be paid to the length scales of mapped variables. The approach in making the sections and maps is described below.

The vertical sections are made by performing a one-dimensional N-S objective map for each vertical level. The assumed covariance is Gaussian, with a correlation length of 5 km. Further, it is assumed that the observation noise is zero so the map is forced to agree with the data at measurement locations. The choices of correlation length and noise are subjective but provide the best horizontal resolution reasonably possible.

In making the horizontal maps, careful attention is paid to the observed length scales. Each vertical level is mapped separately to save computational expense, as opposed to making a fully three-dimensional map. An objective mapping technique [*Le Traon*, 1990] is used in which the mean field is assumed to be described by a set of functions and the statistics of the eddy field are assumed Gaussian. This technique is equivalent to doing an objective function fit to define the mean [*Davis*, 1985], followed by an objective map [*Bretherton et al.*, 1976]. The

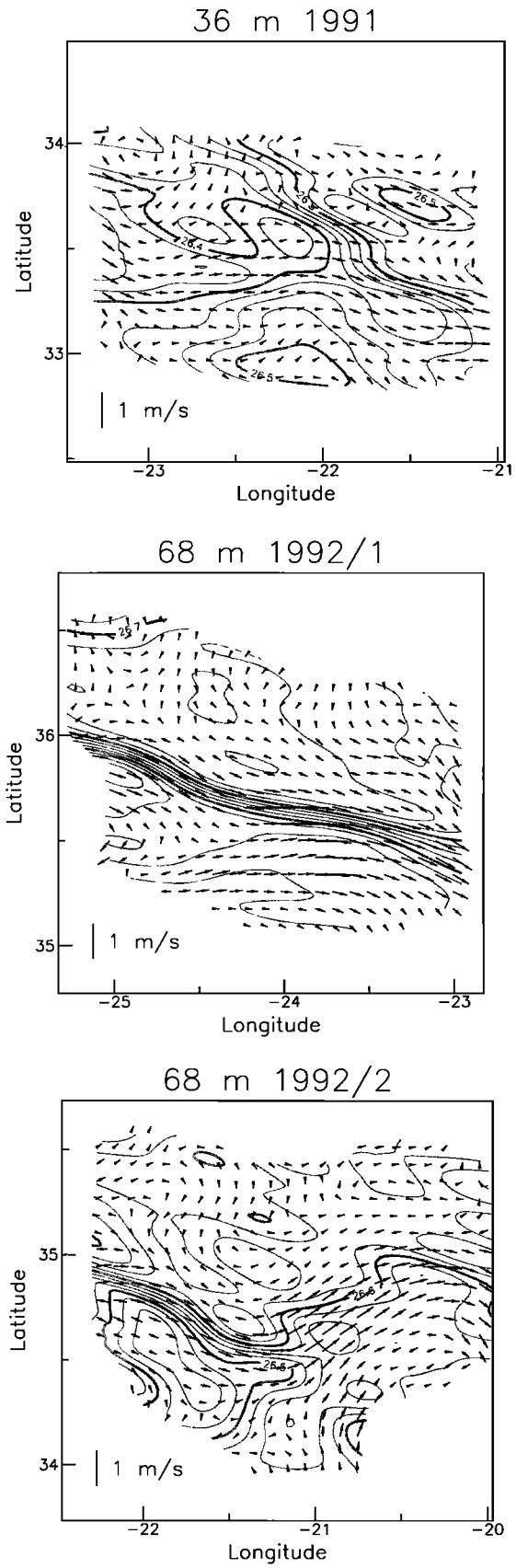

Figure 2. Maps of potential density and velocity plotted as vectors in the mixed layer for the three surveys. The contour interval is 0.025 kg m^{-3}, and the velocity scale is shown. The map is shown only where the mapping error energy is less than 0.3 times the signal.

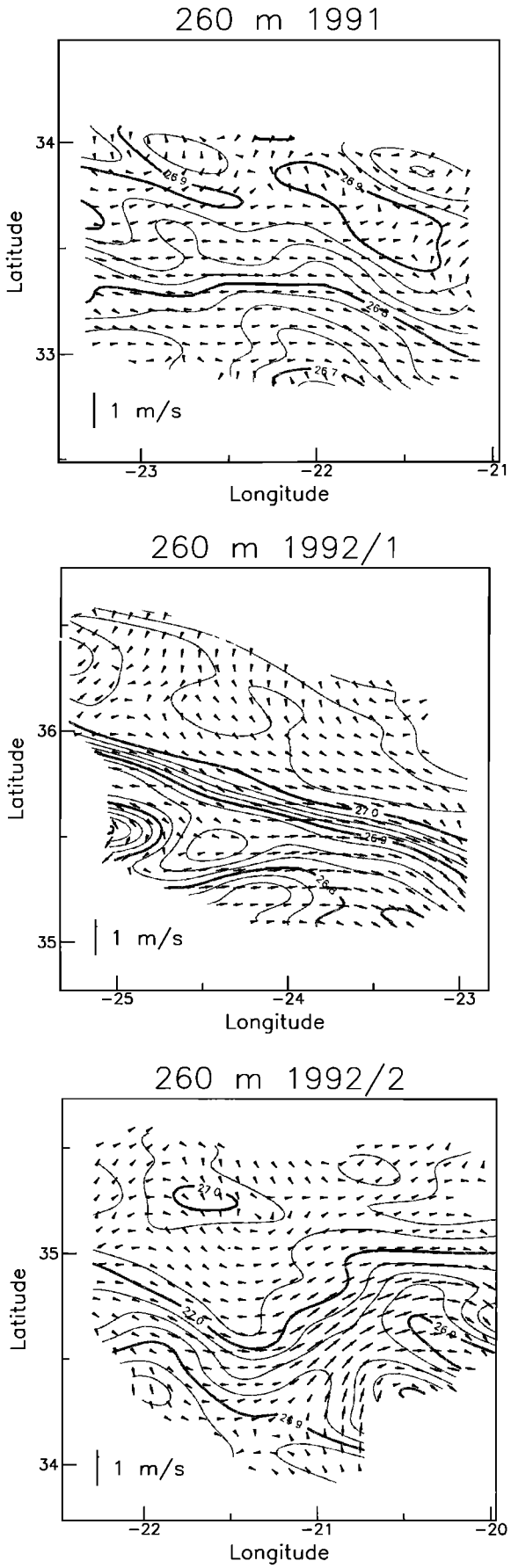

Figure 3. Potential density and velocity in the seasonal thermocline for the three surveys.

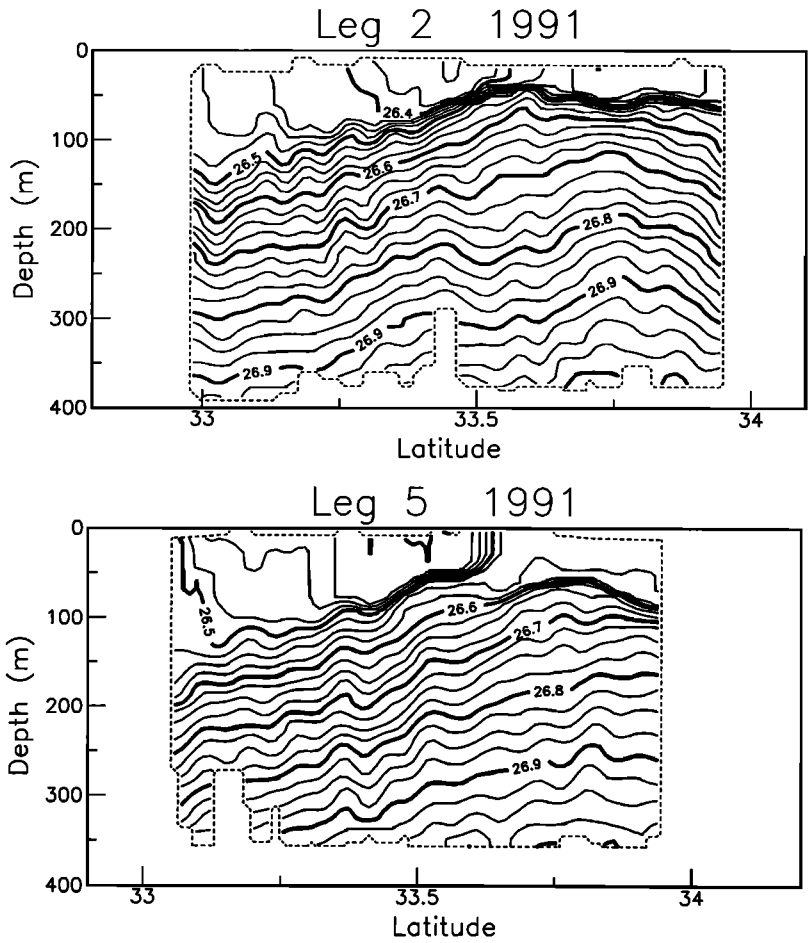

Figure 4. Across-front sections of potential density from the 1991 survey, legs 2 and 5. The contour interval is 0.025 kg m^{-3}. The map is shown only where the mapping error energy is less than 0.3 times the signal.

means were defined to be planar for the hydrographic variables and constant for the velocity. The choice of functions to define the mean fields is consistent with the thermal wind relation, although the fields were not constrained to obey thermal wind. For simplicity, all variables are mapped using a single Gaussian covariance function with an across-front correlation length of 15 km and an along-front correlation length of 50 km, where the across-front direction is 13.2°T. It is assumed that the data include an uncorrelated noise of 0.05 times the signal energy.

The parameters of the covariance were calculated by fitting to the observed covariance estimated in 3.5 km N-S by 25 km E-W bins. The correlation lengths used were the best fit to the potential density autocovariance; correlation lengths for temperature and salinity were slightly shorter, while those for velocity were slightly longer. As a check on the maps, the misfit between the maps and the data was examined to affirm that no coherent variability remained.

4. Hydrography

An initial goal is to obtain a complete description of the Azores Front. We examine potential density, potential temperature, and salinity in individual sections and horizontal maps. An important issue in this section is to determine if tracers support the notion that there is a strong vertical circulation near the front. Compensation of temperature fronts by salinity has been observed in a number of instances, and some theoretical studies exist. In examining the temperature and salinity, we ask if compensation is a feature of the Azores Front.

4.1. Potential Density

The three surveys of the front reveal many similarities but also some striking differences (Figures 2 and 3). Two maps of potential density σ_θ are shown for each survey; one map is chosen to be representative of the mixed layer and one of the seasonal thermocline. For each survey it is possible to identify a region of especially strong horizontal gradients in the mixed layer, but the front during the first 1992 survey (1992/1) is the most striking. In the seasonal thermocline there is a more gradual N-S gradient in density. The very strong gradients during survey 1992/1 are reflected at depth, while the gradients for the other two surveys are weaker.

The surveys consisted of a series of N-S legs on the assumption that the strongest gradients would be in this direction. It is clear from Figures 2 and 3 that this assumption held true at some places better than at others. To the extent that gradients are not in the N-S direction, they will be poorly resolved by the survey. Examples of this phenomenon can be seen in the along-front variation in N-S gradient during surveys 1991 and 1992/1. On the whole, however, the choice of N-S legs was reasonable and gradients were fairly well resolved.

In addition to strong fronts, a few eddies are evident. An example of a warm eddy can be seen in the NE corner of survey 1991 at 260 m (Figure 3), and another is clipped in the SW

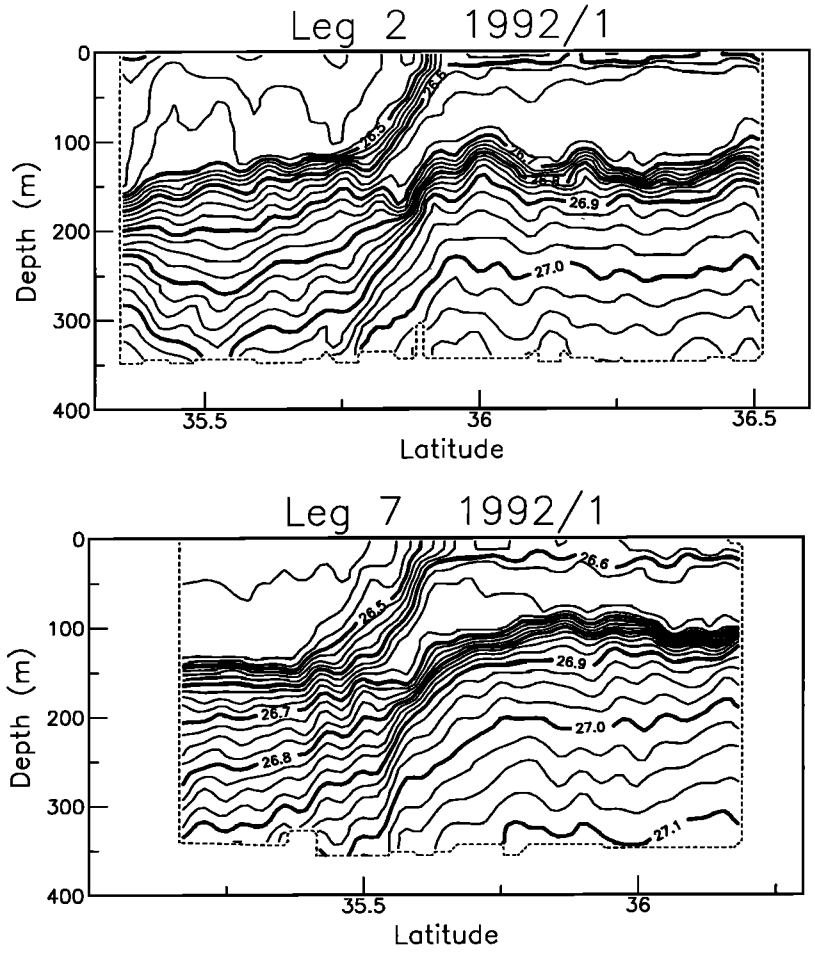

Figure 5. Across-front sections of potential density from survey 1992/1, legs 2 and 7.

corner of survey 1992/1. A weak cold eddy is seen to the east of the warm eddy in survey 1992/1. Theory [*Samelson*, 1993] predicts that cold (positive vorticity) eddies should be preferred. Although we cannot make a definitive conclusion because of the small number of eddies observed, there appears to be no tendency for one sign of eddy to predominate.

There is evidence of streamers extending in the along-front direction. Examples can be seen during each survey, especially in the mixed layer. These streamers are presumably due to the straining of the along-front flow. The streamers are even more apparent in the potential temperature observations discussed below.

Selected across-front sections of potential density from the three surveys show a variety of structures. Consider the three surveys in turn. The 1991 survey was done in May, well after spring warming had already begun (Figure 4). The mixed layer varies in depth from roughly 50 m north of the front to about 100 m south of the front. The dense water to the north of the front penetrates beneath the outcropping isopycnals along leg 5 in a seeming manifestation of subduction. No such penetrating isopycnal can be seen in leg 2, and it is quite difficult even to identify an outcropping front. A warm streamer can be seen south of the front. The seasonal thermocline slopes gently downward to the south beneath the mixed layer.

Survey 1992/1 reveals the strongest front observed (Figure 5). A plunging isopycnal is seen on the dense side of the front in both legs penetrating through the well-defined base of a mixed layer. This subducting isopycnal appears in all legs of this survey. An interesting feature of this survey is the thick homogeneous layer beneath a stratified cap to the north of the front. This survey was done in early March 1992 at the very beginning of spring warming. This cap is the result of a short period of relative calm. A front in the seasonal thermocline accompanies the front in the mixed layer.

Survey 1992/2 (Figure 6) has the most complicated spatial structure, and it is difficult to choose a single front in the mixed layer. Relatively unstratified layers topped by zones of higher stratification can be seen (near 100 m to the north) in both sections. This survey was done later in March, immediately following a small storm which might have mixed away some of the cap seen during the first survey. The storm likely also had an affect on the front in the mixed layer. There are some noticeable undulations in the sub-mixed-layer isopycnals, although the general trend is for a downward slope to the south. Streamers can be seen in the mixed layer once again.

4.2. Potential Temperature

The potential temperature θ is interesting only if its fields are different from those of potential density. The extent to which these fields are different is an indication of the water's "spiciness" [*Munk*, 1981; *Veronis*, 1972]. The spiciness can be seen by comparing potential temperature in the mixed layer (Figure 7) to potential density (Figure 2). In the 1991 survey, for instance, the gradient in θ coincides with a gradient in σ_θ to

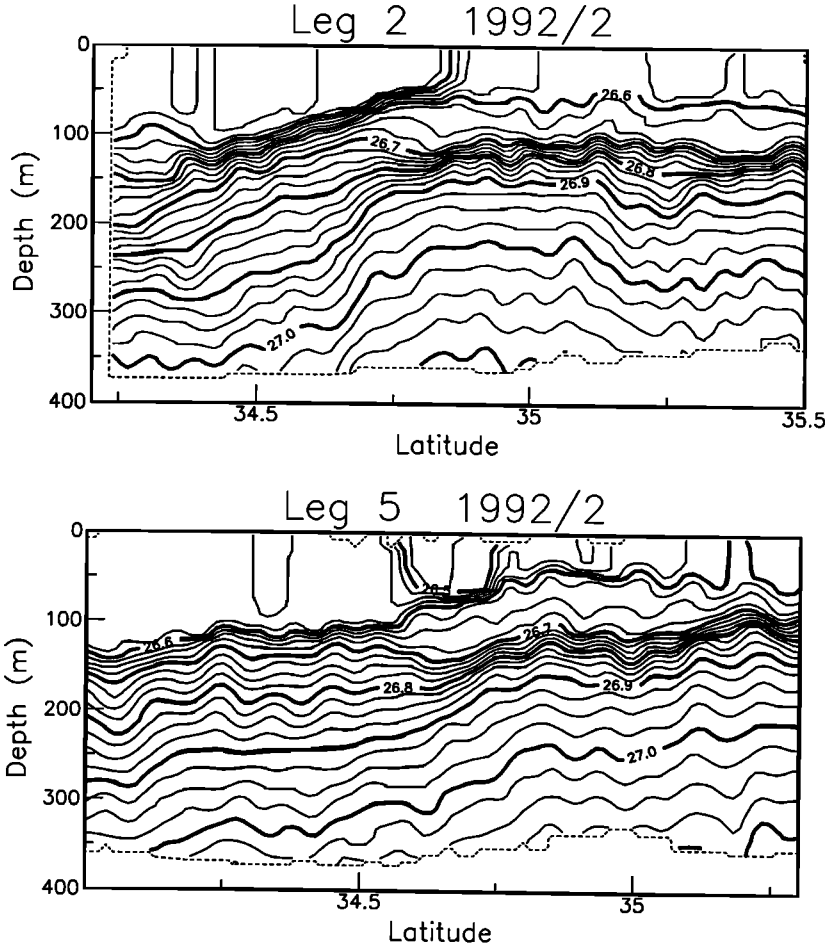

Figure 6. Across-front sections of potential density from survey 1992/2, legs 2 and 5.

the east, while the θ gradient to the west is compensated by salinity. There are streamers in θ to the north of the front during survey 1992/1 that do not appear in σ_θ. In survey 1992/2, salinity causes the strength of the front in σ_θ to vary with along-front position. Isotherms and isopycnals follow each other closely beneath the mixed layer so deeper maps of θ are not shown.

The θ streamers can be seen more clearly in individual sections. The most striking example can be seen in survey 1992/1 (Figure 8), where a θ streamer to the north of the front does not appear at all in σ_θ. A feature of all of these fronts is that the subducting isopycnal is spicy. A close examination of leg 5 in 1991 reveals that isotherms and isopycnals are nearly orthogonal in the apparently subducting region under the front. To some extent, the same situation can be seen in the subducting layer of leg 2 survey 1992/2.

4.3. Potential Temperature-Salinity Plots

The spiciness of individual isopycnals can be viewed in θ-S plots (Figure 9). Just as the front in survey 1992/1 is the simplest in physical space, it is also most the striking in θ-S space. A few features are readily apparent as follows: (1) the gap near $\sigma_\theta = 26.5$ kg m^{-3} is the manifestation of the front, (2) spiciness is seen along the subducting isopycnal in the range 26.6–26.7 kg m^{-3}, and (3) there is much less spiciness in the seasonal thermocline. These same features can be seen in the other two surveys to a greater or lesser extent. The gap indicative of the front is more pronounced in 1991, and the θ-S relationship is even tighter at depth. However, the spiciness is less apparent because the front is weaker and the mixed layer is thinner. The front in survey 1992/2 is more complicated, and the gap in θ-S space is less obvious. There is clearly more spiciness in the mixed layer than at depth, but a bit of anomalously salty water is seen near $\theta = 14$°C. This water was seen on all but two of the legs on the southern side of the survey so it cannot be dismissed as instrument error. All we can say is that we managed to clip the edge of an intrusion from the south.

5. Velocity and Dynamics

The goal in examining the velocity field is to make simple inferences about the heat and momentum balances. The heat balance can be addressed simply by determining how nearly isopycnal is the horizontal flow. The thermal wind balance is studied through independent observations of density and vertical shear. Finally, the density and velocity fields are used to map the dynamical tracer potential vorticity.

5.1. Horizontal Velocity

The horizontal velocity in the mixed layer (Figure 2) approaches 0.5 m s^{-1} and is generally along isopycnals, especially during survey 1992/1. This infers that the sum of rate of change and vertical advection of density must be small. If the horizontal flow crosses isopycnals, either a vertical velocity or a tem-

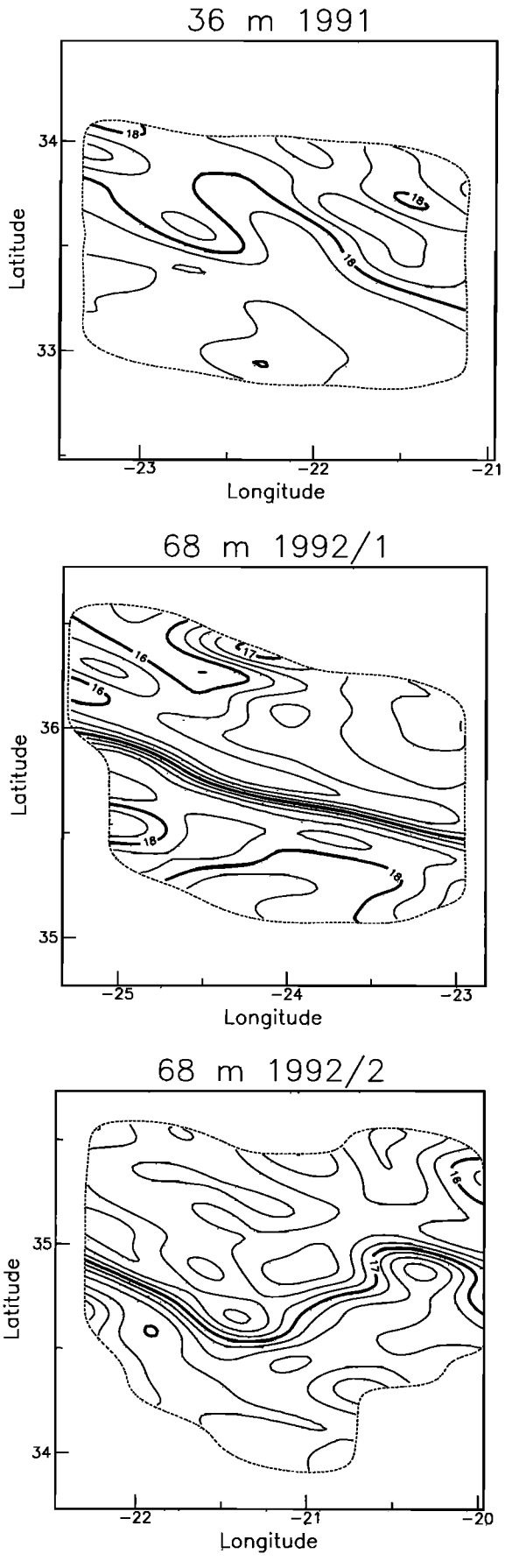

Figure 7. Maps of potential temperature in the mixed layer from the three surveys. The contour interval is 0.25°C.

poral change is indicated. Assuming the velocity is in geostrophic balance (an assumption that will be tested below), the flow in the mixed layer should be a vertical integral of density gradients from a level of no motion somewhere deep in the water column. Density gradients in the mixed layer may not be normal to the velocity. This may help to explain why the flow may sometimes cross isopycnals and form streamers.

The cause of some of the velocity features in the mixed layer are revealed in the seasonal thermocline (Figure 3). The eddies in the NE corner of survey 1991 and in the SW corner of 1992/1 can be easily identified. Still, there are regions where the flow is across isopycnals and the heat balance cannot be purely horizontally advective. The velocity at this depth peaks near 0.3 m s^{-1}, smaller than in the mixed layer, consistent with the thermal wind relation and a deep level of no motion.

Sections give a clearer picture of the vertical structure of velocity (Figure 10). The core of high eastward velocity can be identified on the warm side of the front in every survey. This behavior is again consistent with thermal wind, since it is the shear which should coincide with the front, and the velocity at the surface is a vertical integral of shear over several hundred meters. Note that we have not reached the bottom of the eastward flowing current, even with our deepest measurements of over 300 m. The horizontal structure of velocity is somewhat noisier in 1992 than in 1991. We believe this is a result of the degraded navigation in 1992; the additional smoothing in the horizontal maps (Figures 2 and 3) filters this noise to a great extent.

5.2. Shear and Thermal Wind

It is reasonable to ask how well the thermal wind relation is satisfied. At issue is not whether the thermal wind relation is valid in the ocean, since it must be a first-order description for large scales and with sufficient averaging. It is of interest to see if we can resolve the shear due to thermal wind in the presence of strong near-inertial shear. The vertical shear of eastward velocity is shown in Plate 1. Where the front slopes most strongly in the mixed layer, there is high shear of the sign required by thermal wind. This shear is quite apparent in survey 1992/1 which has the strongest front, is less obvious in 1991, and is a bit hard to see in survey 1992/2. Shears in other locations are not balanced by horizontal density gradients. In particular, shear at the base of the mixed layer in all surveys is likely to be due to near-inertial internal waves. It is interesting to note that the shears in the subducting isopycnals tend to be small.

A measure of the agreement with the thermal wind relation is given by a regression of shear against horizontal density gradient. If the thermal wind balance were exact, then the shear would be related to the density gradient as

$$u_z = \frac{-ig}{f\rho_0} \nabla\rho, \tag{1}$$

where the velocity shear u_z and density gradient $\nabla\rho$ are written as complex variables, with the eastward component the real part and the northward component the imaginary part, i is the square root of -1, g is the acceleration due to gravity, f is the Coriolis parameter, and ρ_0 is a reference density. Consider a linear model in which the estimate of the vertical shear is

$$\hat{u}_z = a \frac{-ig}{f\rho_0} \nabla\rho \tag{2}$$

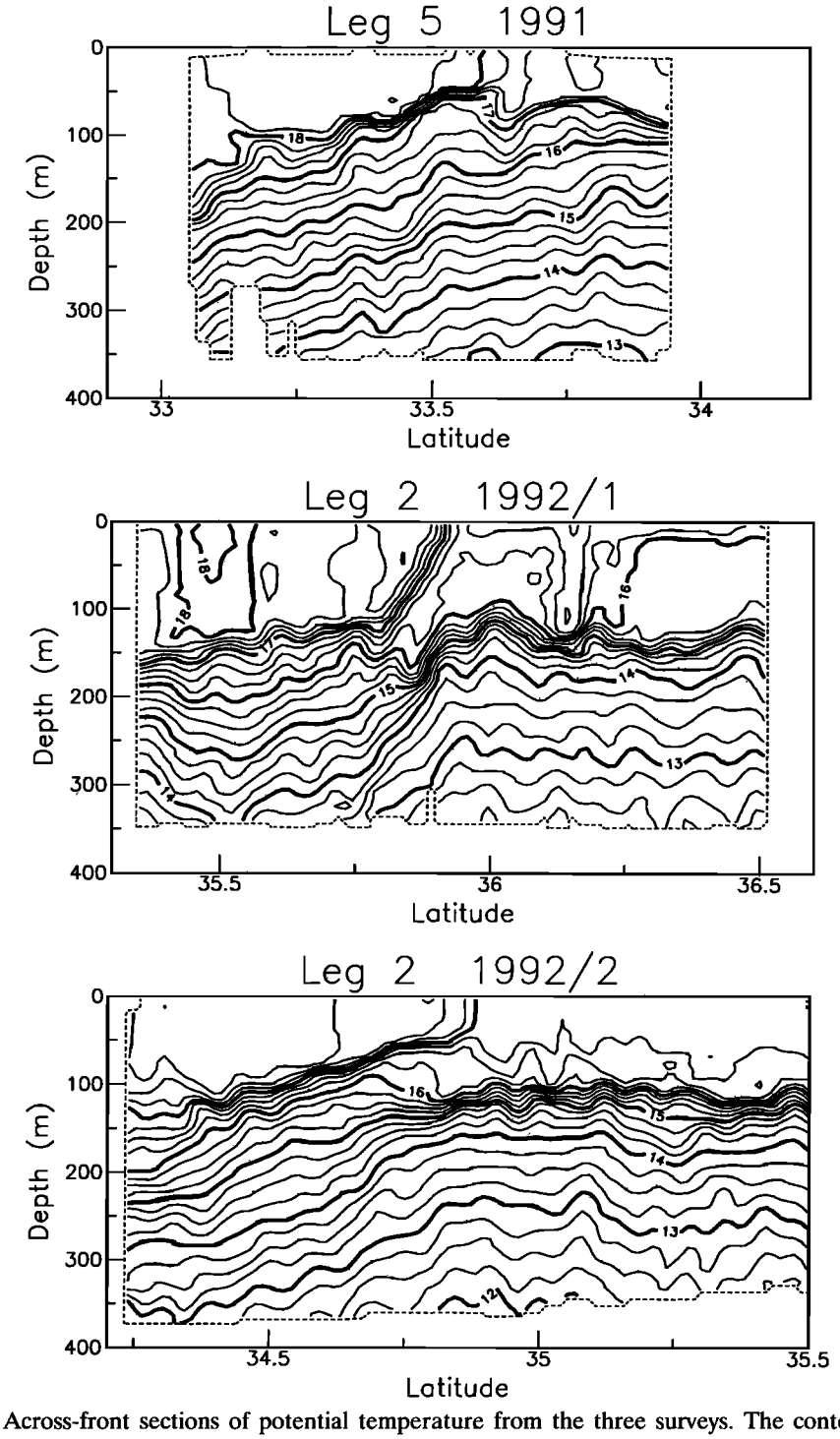

Figure 8. Across-front sections of potential temperature from the three surveys. The contour interval is 0.25°C.

and a is a constant to be determined. The regression constant that results in the smallest mean square error between the observed and modeled velocity shear is

$$a = \frac{if\rho_0}{g} \frac{\langle u_z \nabla \rho^* \rangle}{\langle \nabla\rho \nabla\rho^* \rangle} \tag{3}$$

where the angle brackets denote an ensemble average and the asterisk indicates the complex conjugate. Agreement with thermal wind is evaluated by how close a is to the theoretical value of 1.

The regression coefficient a is calculated (Table 1) with the ensemble defined to be the grid points of the three-dimensional maps where the ratio of error-to-signal variance is smaller than 0.3. The tendency is clearly for the shear to be in the direction appropriate for thermal wind. The agreement is remarkably good for the 1992/1 survey which had the strongest and straightest front. While the direction of a is very close to the theoretical value for the other two surveys, the magnitude is low. This is just the sort of behavior one would expect if the density gradient were noisy, increasing the magnitude of the

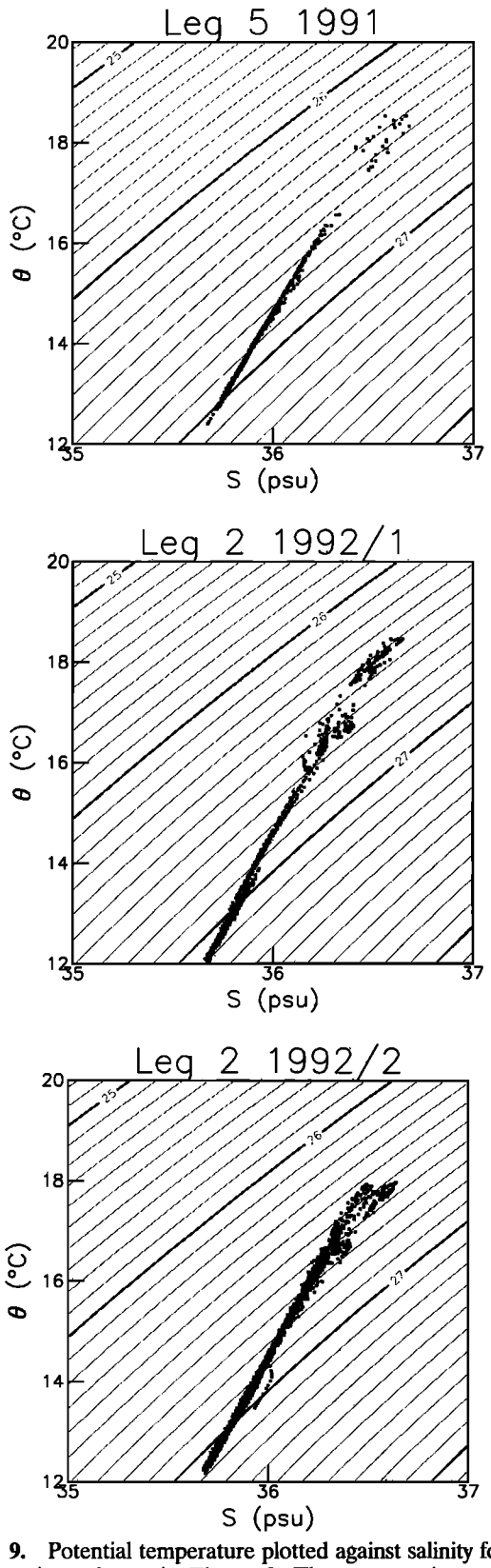

Figure 9. Potential temperature plotted against salinity for the three sections shown in Figure 8. The contour interval for potential density is 0.1 kg m^{-3}.

denominator in (3) without changing the numerator or the phase of the result. The fronts in 1991 and 1992/2 were more variable in direction than in 1992/1, and the density gradient is noisier because the sections are not as nearly across the fronts.

Table 1. The Regression Coefficient a Defined by Equation (3) Describing Velocity Shear in Thermal Wind Balance, Correlation Coefficient, and Error

Survey	Magnitude	Phase, deg	Correlation	Error
1991	0.64	2.3	0.16	0.55
1992/1	0.95	−1.1	0.29	0.30
1992/2	0.70	4.5	0.18	0.51

If the thermal wind balance were exact, then a would have a magnitude of 1 and a phase relative to the real axis of 0°. The 1-standard-deviation error (calculated assuming 60 degrees of freedom) applies to either magnitude or phase measured in radians.

These low values of a are likely a result of poorly resolved eastward density gradients. The correlation coefficients for the three surveys are not high, reflecting the amount of shear due to internal waves. The correlation varies in the vertical, having a maximum in the mixed layer where the front is strongest, a minimum at the mixed-layer base where near-inertial shears are large, and a smaller maximum in the seasonal thermocline. The error is calculated under the assumption that we have 60 degrees of freedom, 20 in the horizontal (consistent with the length scales used for the maps) and 3 in the vertical.

5.3. Potential Vorticity

A useful tracer conserved in the absence of mixing is Ertel's potential vorticity defined as

$$q = -\rho_0^{-1}(f\hat{\mathbf{z}} + \zeta) \cdot \nabla\sigma_\theta, \tag{4}$$

where ζ is the relative vorticity, $\hat{\mathbf{z}}$ is a unit vector directed upward, and the horizontal component of planetary vorticity has been neglected. Given three-dimensional fields of potential density and horizontal velocity, q can be approximated as

$$q_3 = -\rho_0^{-1}\left[\left(f + \frac{\partial v}{\partial x} - \frac{\partial u}{\partial y}\right)\frac{\partial \sigma_\theta}{\partial z} - \frac{\partial v}{\partial z}\frac{\partial \sigma_\theta}{\partial x} + \frac{\partial u}{\partial z}\frac{\partial \sigma_\theta}{\partial y}\right], \tag{5}$$

where horizontal gradients in the vertical velocity have been neglected. Further assuming that along-front gradients may be neglected, the potential vorticity may be approximated using individual sections by

$$q_2 = -\rho_0^{-1}\left[\left(f - \frac{\partial u}{\partial y}\right)\frac{\partial \sigma_\theta}{\partial z} + \frac{\partial u}{\partial z}\frac{\partial \sigma_\theta}{\partial y}\right], \tag{6}$$

where it is assumed that the coordinate y is in the across-front direction. The validity of this approximation is affected by how nearly across-front the section is.

Using (6), the total potential vorticity, the planetary vorticity component, and the component due to the vertical shear (the tilting term) are calculated for the second leg of survey 1992/1 (Plate 2). The potential vorticity tends to be near zero in the mixed layer because there are no density gradients. In the seasonal thermocline, q is about 0.1×10^{-9} m^{-1} s^{-1} and is due almost entirely to the vertical gradient of density. The potential vorticity is highest in the base of the mixed layer where it may be modulated, to some extent, by the relative vorticity. The subducting isopycnal carries with it the low potential vorticity of the mixed layer, and water could be moving downward along this isopycnal while conserving q. The tilting term is greatest by far in the front, where it is of a sign to reduce the magnitude of q. This is precisely the behavior one would expect if the front were in thermal wind balance, in which case the tilting

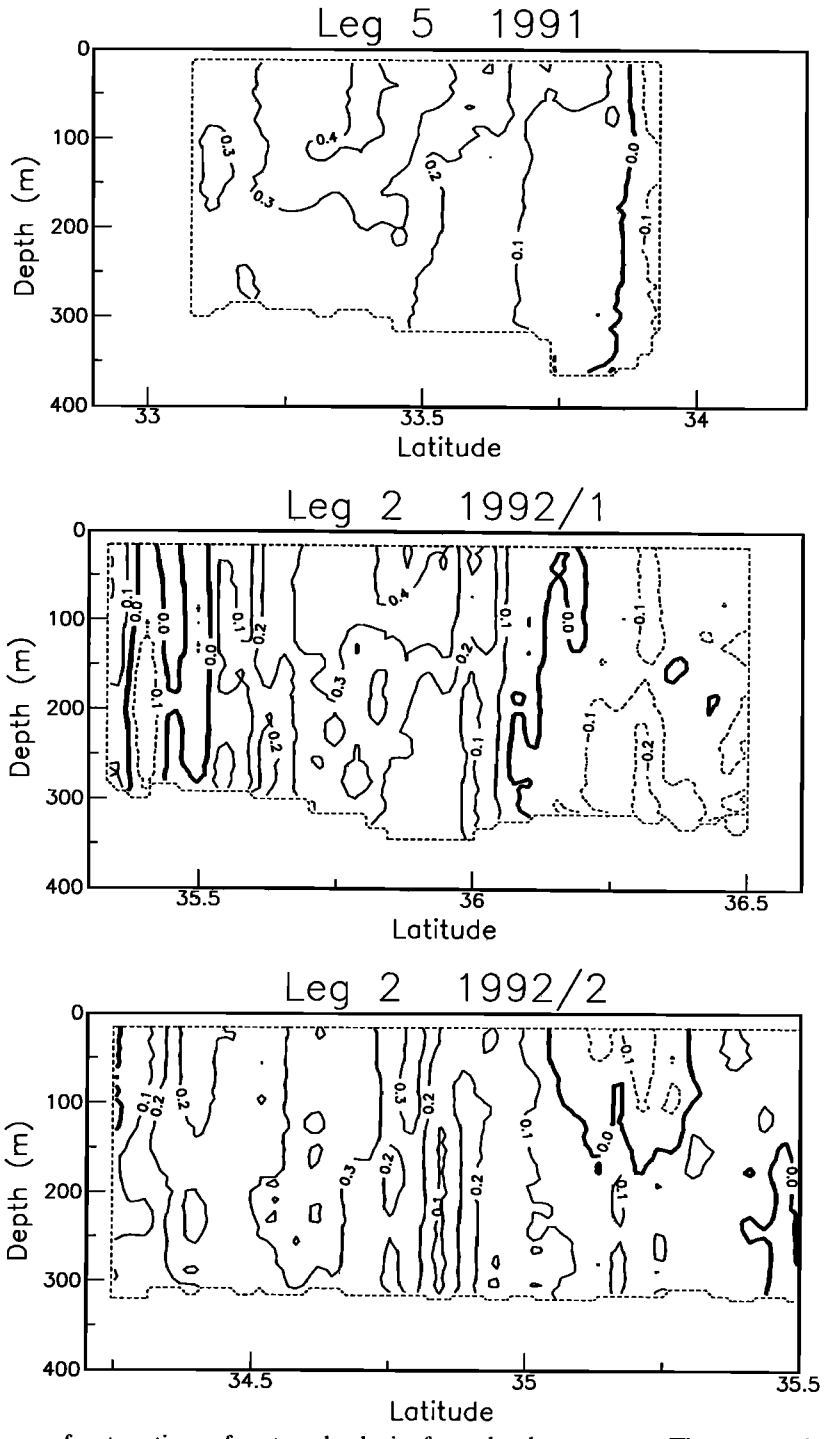

Figure 10. Across-front sections of eastward velocity from the three surveys. The contour interval is 0.1 m s^{-1}.

term should always be opposite in sign to the stretching term. The magnitude of the tilting term in the mixed-layer front is roughly the same as the total vorticity in the seasonal thermocline. If the shear were in thermal wind balance, the tilting term could only be underestimated by neglecting the across-section gradients, and our estimate of q in the front is likely high. Low q across the front implies also that the Richardson number is low because of the increased shear, and mixing may be enhanced in the frontal zone.

It is interesting to compare these results to the seminal two-dimensional model of *Hoskins and Bretherton* [1972]. The model describes the evolution of an inviscid fluid with zero potential vorticity and a very small initial horizontal density gradient. Because of strain placed on the fluid, the density gradient grows while q must remain zero. The result in the semigeostrophic approximation is an infinitely sharp front in a finite time. A simple interpretation of zero potential vorticity is that the absolute vorticity must be parallel to isopycnals, as is the tendency in the observed front. However, the potential vorticity is not exactly zero across the observed front. This

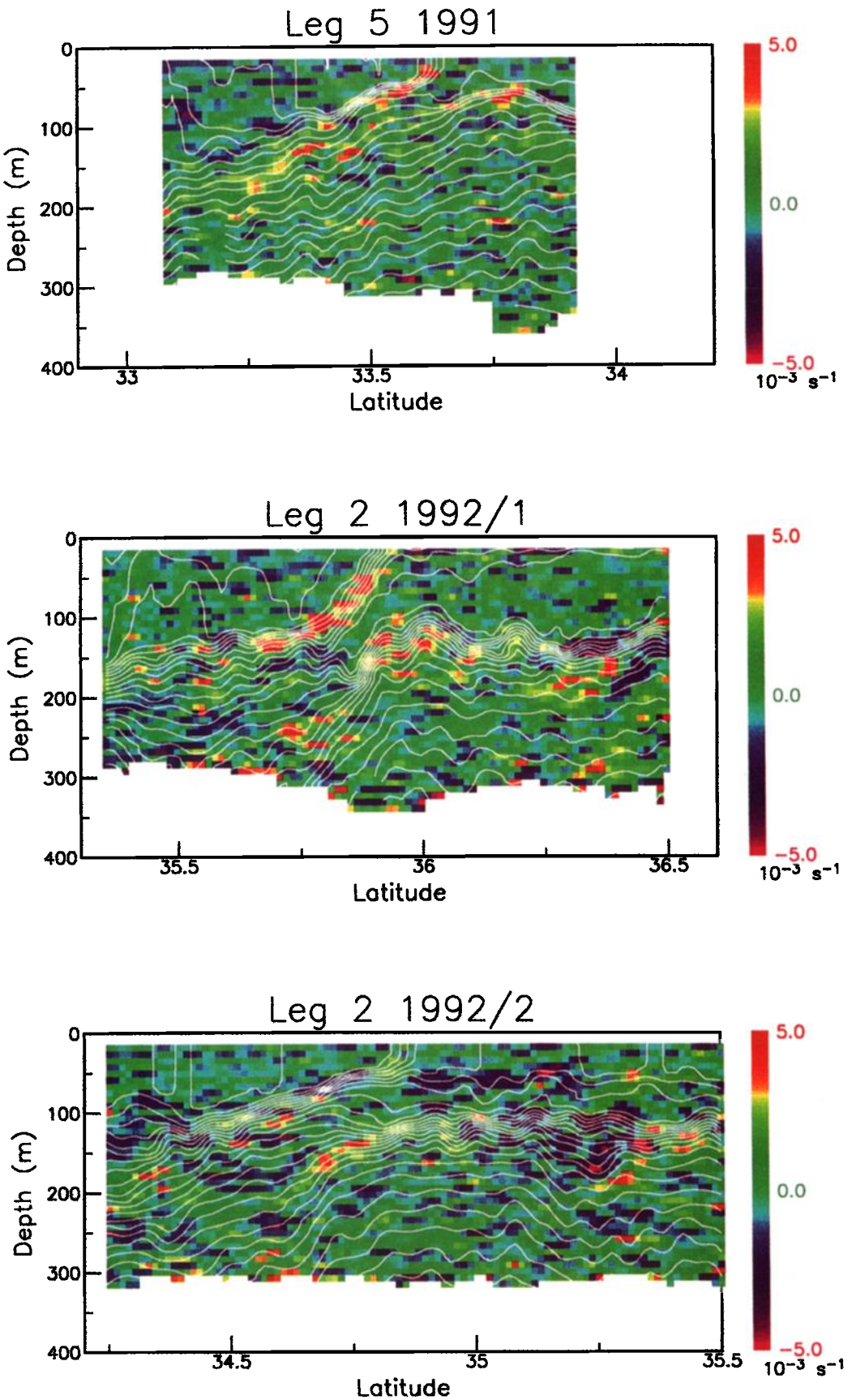

Plate 1. Across-front sections of the vertical shear of velocity plotted as a color image. The scale is shown on the right. The white lines are isopycnals as in Figures 4–6. Note the high shear in the region of the front.

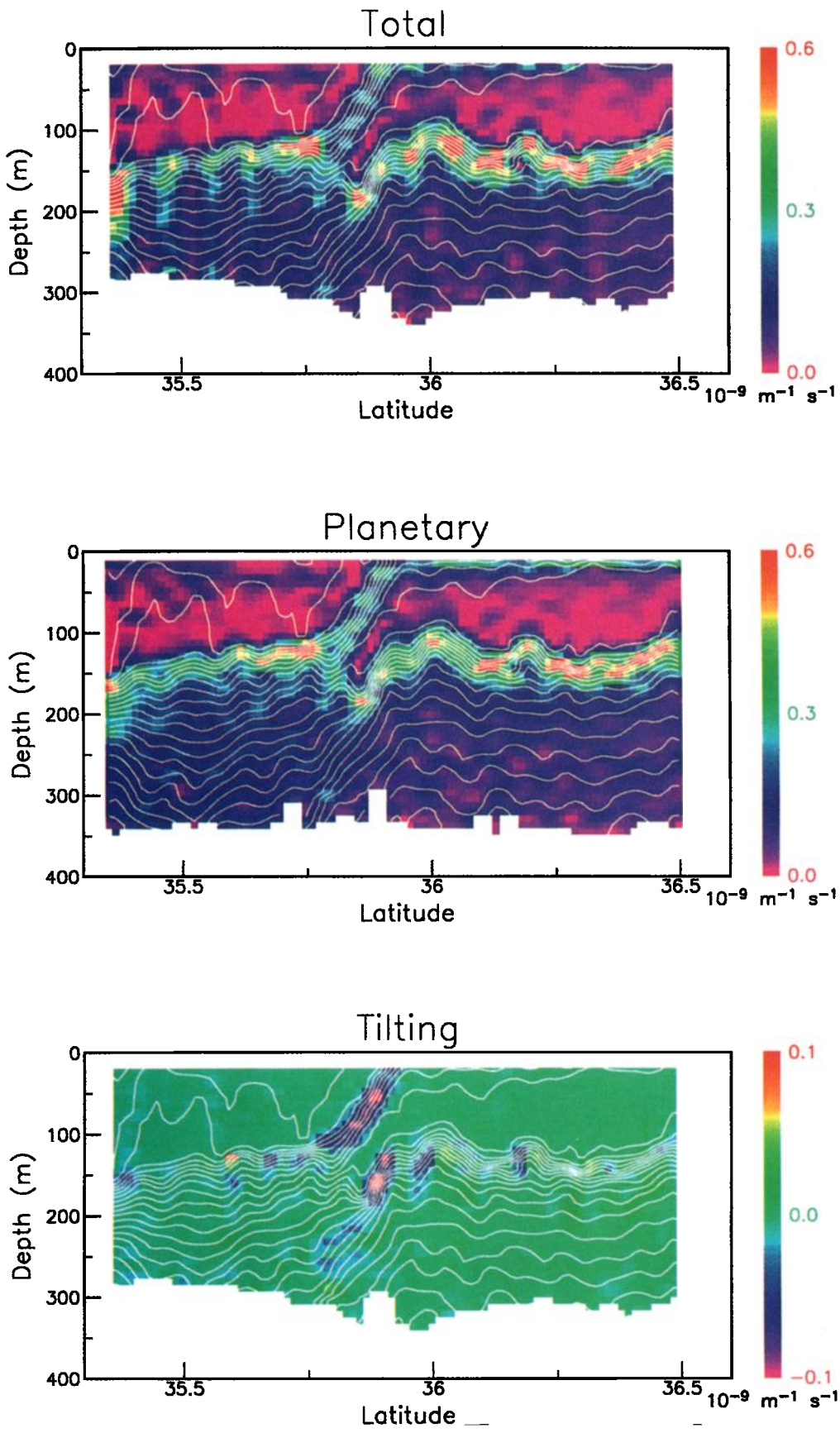

Plate 2. Across-front sections from leg 2 of survey 1992/1 of (top) the total potential vorticity assuming along-front gradients are negligible, (middle) the component due to planetary vorticity, and (bottom) the component due to vertical shear. Note the change in scale on the bottom section. The white lines are isopycnals.

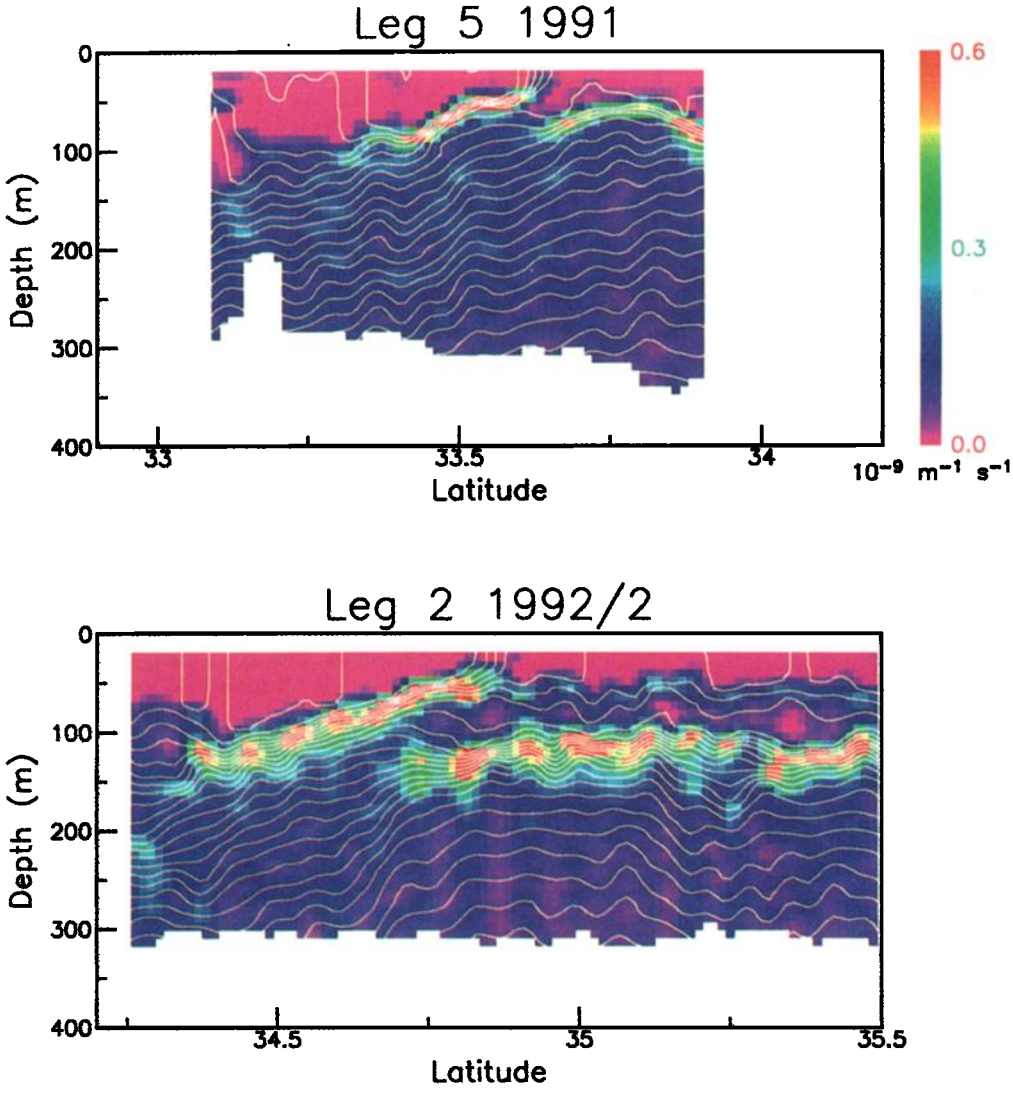

Plate 3. Across-front sections of the total potential vorticity assuming along-front gradients are negligible for leg 5 of survey 1991 and leg 2 of survey 1992/2.

could be due to internal-wave shear or mixing, neither of which is represented in the model.

Sections of potential vorticity from the other two surveys show some of the same features (Plate 3). In all cases the subducting isopycnal is also a layer of low potential vorticity. The potential vorticity stays low across the front in the mixed layer in all surveys. In all cases the base of the mixed layer is a local maximum in q because of high vertical density gradients. The potential vorticity at depth is near 0.1×10^{-9} m^{-1} s^{-1} in all surveys. It should be noted that the two-dimensional approximation (6) may not be as good for these surveys because of greater along-front variability.

Maps of the potential vorticity, using (5), in the mixed layer demonstrate that q usually, but not always, remains low across the front (Plate 4). This is quite clear in survey 1992/1 which has the strongest and straightest front. A similar picture is seen in 1991, except for two regions of higher q, where the base of the mixed layer intersects the depth of the map. Survey 1992/2 has a more interesting structure in that there is a noticeable change in potential vorticity across the front. The 68-m depth is in the surface mixed layer south of the front but in a slightly stratified layer beneath the surface mixed layer north of the front. Again, regions of high q are associated with the base of the mixed layer shoaling. Note that the highest values of q may be lower in the horizontal maps than in the sections because the maps are smoother.

6. Discussion and Conclusions

This study has revealed a number of descriptive features of the Azores Front, many of which should be seen at other oceanic fronts. The hypothesis that there is subduction on the dense side of the Azores Front is supported by such tracers as potential density and potential vorticity. There is clear evidence that the subducting isopycnal tends to be spicy in the sense that there is θ-S variability. The potential vorticity is reduced across the front because of the component of vorticity in the direction of the horizontal density gradient. The thermal wind balance is valid, especially in the region of the front in the mixed layer. The horizontal flow is very nearly along isopycnals, indicating that the rate of change and vertical advection

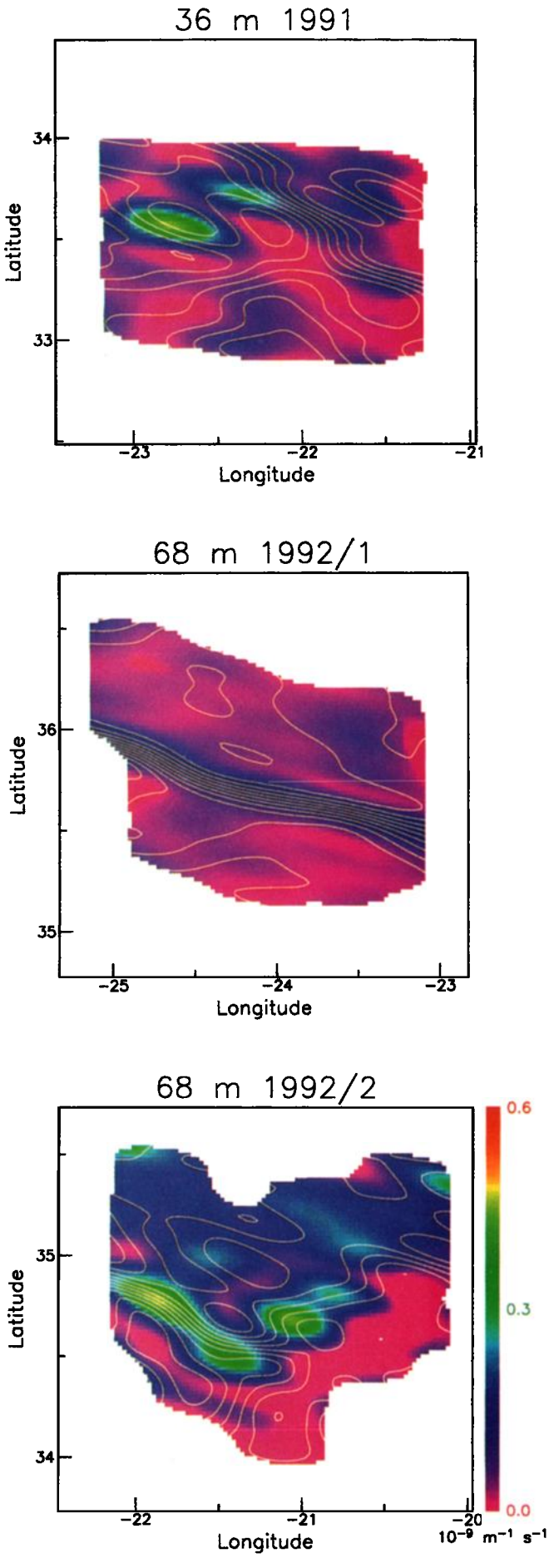

of density must be small. The implications of these observations are discussed below.

The fields of potential density and potential vorticity support the notion that there is subduction on the dense side of the front. Since these tracers are at least approximately conserved in the absence of mixing, identifying layers of uniform σ_θ and q is suggestive that subduction could be occurring. We have thus far presented no proof that flow is actually downward along the apparently subducting isopycnal, and the subducting layers could be the result of a previous event. It must be emphasized that the flow is very nearly horizontal and any vertical flow must be small. We will address the issue of the rate of the subduction process in part 2 [*Rudnick*, 1996].

That the subducting isopycnal tends to be more spicy than isopycnals in the seasonal thermocline seems to be a general feature. Compensation of temperature gradients by salinity is often observed [*Flament et al.*, 1985; *Roden*, 1980]. Just as the subducting isopycnal is spicy, the front is also somewhat compensated, as can be seen in the θ-S plots (Figure 9). An example of compensation in a theoretical model is presented by *MacVean and Woods* [1980] in an oceanic application of *Hoskins and Bretherton* [1972]. The cause of the compensation in the model is that the isopycnals are spicy in the initial conditions. Since the flow in this inviscid model is primarily along isopycnals, gradients in temperature and salinity increase faster than gradients in density. It is quite possible that this simple explanation is valid for the observations presented here. The phenomenon of compensation of horizontal gradients may be a general feature of all mixed layers and not just frontal zones; further observational study is warranted.

Even in the presence of strong shear due to internal waves, the thermal wind relation tends to be satisfied. Disagreement with thermal wind is more likely due to noisy density gradients rather than any systematic difference in the dynamics. We did not begin this study under the assumption that geostrophy needed to be affirmed by observation, however, we consider Plate 1 (middle) to be a textbook example of thermal wind at relatively small scales. That thermal wind is valid will allow us to infer the geostrophic velocity and the vertical velocity in part 2 [*Rudnick*, 1996].

It is perhaps unsurprising that the horizontal flow is mostly along isopycnals. Were it not so, large changes in density and/or strong vertical circulations would be a necessary consequence. The degree to which the horizontal velocity is parallel to isopycnals may be indicative that the observed fields are reasonably well resolved. To be sure, there are regions where the flow is across isopycnals, and other terms must be important in the heat balance.

The observation that potential vorticity is nearly constant across the front is perhaps the most interesting dynamically. It is reminiscent of the *Hoskins and Bretherton* [1972] model of the evolution of a zero q layer. That observations show similar characteristics may be evidence that the dynamics of Hoskins and Bretherton are applicable. At least, the importance of the tilting term in the potential vorticity must be acknowledged in frontal regions. The increased shear in the frontal zone forces the Richardson number to remain low, indicating possibly enhanced mixing. Estimates of potential vorticity in a frontal

Plate 4. (opposite) Maps of the potential vorticity in the mixed layer from the three surveys. The white lines are isopycnals.

zone have been presented by *Pollard and Regier* [1990, 1992], who emphasized the large variations in q evident in the mixed-layer base (Plates 3 and 4). These are due to changes in the stratification and relative vorticity. Here the emphasis is on the lack of variation in the mixed-layer q because of increased shear at the front.

The main unanswered question at this point is the rate of the subduction process. The vertical velocity was not directly measured and can only be inferred from the observations using assumed dynamics. This is an inverse problem whose solution is deserving of careful treatment and will be presented in part 2.

Appendix: CTD, GPS, and ADCP Data Processing

A1. Conductivity-Temperature-Depth

The CTD data require correction for the different response times of the conductivity and temperature sensors. A simple model of the temperature response is

$$\tau \frac{d\hat{T}(t)}{dt} + \hat{T}(t) = T(t - L), \tag{A1}$$

where T and $\hat{T}$ are true and measured temperature, t is time, L is a lag, and τ is the response time of the thermistor. The model takes into account that, first, the thermistor is located downstream of the conductivity sensor, and second, the thermistor responds more slowly to a change of temperature than the conductivity sensor.

Correcting the response of the thermistor is easiest to do in frequency space. The effect of a lag (nonzero L) is a change in phase with no change in amplitude. A single-pole filter (nonzero τ) is equivalent to a lag at low frequency but amplifies with increasing frequency while asymptoting to a phase of $\pi/2$, thus having the effect of introducing high-frequency noise. The cross-spectrum between the measured temperature and conductivity is calculated using the 24-Hz raw data from deeper than 200 dbar, where the temperature-salinity relationship is fairly tight. The phase is then fit, yielding the values $\tau = 2.3$ scans (where a scan is the raw sampling period of 1/24 s) and $L = 3.8$ scans and correcting the phase up to a frequency of 6 Hz. Since a typical vertical profiling speed is 1 m s^{-1}, this corresponds to a vertical resolution of 1/6 m. Applying only a lag correction of 6 scans corrects the phase up to a frequency of 1 Hz for 1-m resolution. Since the final product is 8-m bins, the simple lag correction is adequate and much simpler to implement. Temporal averaging over a full cycle of the vehicle's path further minimizes errors due to temporal mismatches of the sensors.

Errors caused by the thermal mass of the conductivity cell are discussed by *Lueck* [1990]. *Lueck and Picklo* [1990] demonstrate the effect as a density inversion at the interface between two well-mixed layers in temperature. *Morison et al.* [1994] show the effect as an offset between temperature-salinity curves for the upward and downward casts. Neither symptom is apparent in our data, and no correction is made. The effect decreases with increasing flushing rate and decreasing rate of change of temperature. Since our tow speed (and therefore flushing rate) is 4 m s^{-1} and our vertical profiling speed is 1 m s^{-1}, the effect is expected to be smaller than in any of the studies referenced above.

A2. Navigation

The goal in the initial processing is to identify the noise in the data and to devise an appropriate filter to extract the signal. This goal is easily achieved for 1991, since because of the Gulf War, selective availability (SA) was turned off. The GPS data are of very high quality, and the noise floor is clearly identifiable (Figure A1). The data are so good, in fact, that the roll of the ship is seen as a peak in the spectrum at a period of about 10 s. A reasonable filter to remove the noise is to low pass at the frequency where the signal meets the noise floor. For 1991 this frequency is one cycle per minute.

Unfortunately, SA was turned on for 1992 and the noise floor was much higher (Figure A1). In addition, the noise was apparently nonstationary so that none of the standard linear methods of noise removal could have been expected to work well. Our approach was simply to low pass at a frequency of one-third cycle per minute. Since the noise was not stationary, there were times when the navigation (and thus absolute velocities derived from the ADCP) was noticeably poor. We could come up with no algorithm that would reliably identify such bad navigation while retaining actual small-scale features in velocity. At the level of smoothing shown in this paper, such errors in velocity are, fortunately, small and infrequent.

A3. Acoustic Doppler Current Profiler

The raw ADCP data were collected in 5-min ensembles and 8-m bins, and heading was determined from the ship's gyrocompass. The challenge in calibrating the data is in determining the offset in the heading of the transducer relative to the ship and the error in sound velocity. Methods used in this determination have included the minimization of the difference in calculated velocity over a repeated ship track [*Joyce*, 1989] and minimization of this difference in the vicinity of a change of course [*Pollard and Read*, 1989]. We present a framework which would allow either of these approaches but suggest an alternate measure for selecting the calibration parameters.

Writing the horizontal velocity as a complex variable, where the eastward velocity is the real part and the northward velocity the imaginary part, the correction desired can be written:

$$\hat{u}_s = \gamma u_s, \tag{A2}$$

where u_s is the measured velocity relative to the ship, γ is a complex number to be determined, and the hat refers to the corrected velocity. Since the velocity relative to the Earth u_e is the sum of u_s and the velocity of the ship relative to the Earth U, the corrected velocity relative to the Earth is

$$\hat{u}_e = \gamma u_s + U. \tag{A3}$$

The goal is to determine γ by minimizing some measure of the error that would be caused by a misaligned transducer head or inexactly known sound velocity.

Now consider u_s, u_e, and U for all ensembles and all depths as vectors $\mathbf{u}_s$, $\mathbf{u}_e$, and $\mathbf{U}$. The measure of the error ε can be generalized as a norm of $\hat{\mathbf{u}}_e$,

$$\varepsilon = \hat{\mathbf{u}}_e^H \mathbf{W} \hat{\mathbf{u}}_e, \tag{A4}$$

and minimizing ε with respect to γ yields the result

$$\gamma = -\frac{\mathbf{u}_s^H \mathbf{W} \mathbf{U}}{\mathbf{u}_s^H \mathbf{W} \mathbf{u}_s}. \tag{A5}$$

The matrix $\mathbf{W}$ can be chosen to emphasize a range of depths (a reference layer), to minimize a difference between successive occupations of the same section, or to minimize differences in velocity at the beginning and end of a change in course. Minimizing a difference increases the dependence of γ on small

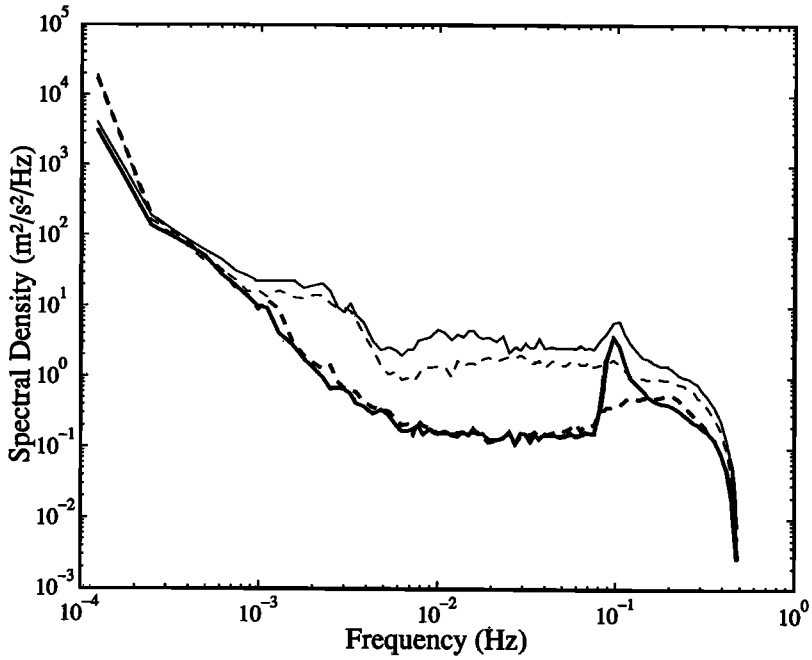

Figure A1. Spectra of Global Positioning System–derived ship's velocity; thick and thin lines are from 1991 and 1992, respectively; solid and dashed lines are eastward and northward velocity, respectively. Note the difference in the noise floors and the peak near 0.1 Hz due to roll in 1991 eastward velocity. The roll peak is in eastward velocity because the surveys consist of a sequence of N-S legs.

space scales and timescales where navigation errors are more severe. Weighting changes in course more heavily introduces errors traceable to the ship's gyrocompass. Our choice is simply to minimize the variance in the velocity relative to the Earth over a reference layer from 48 to 168 m. For this choice, **W** has ones in the appropriate bins and zeros elsewhere.

The estimate (A5) is the negative of the regression of the ship's velocity on the velocity relative to the ship in the reference layer. This method essentially rotates the velocity relative to the ship into a coordinate system fixed to the ship. The calibration constant γ is a normalized average of this rotated velocity. As long as the true water velocity is incoherent with the ship's velocity (as would be the case when a series of turns are made over a slowly evolving velocity field), this method gives a robust estimate for γ.

The calibration constant γ is calculated independently for the two cruises. The magnitude and phase of γ are 1.004 and $-1.05°$ for the first cruise and 0.995 and $-0.96°$ for the second. Because the method is equivalent to a regression, known formulas may be used to estimate the error [*Bendat and Piersol*, 1986]. For the first cruise the correlation-squared between U and u_s is 0.996, and conservatively assuming one degree of freedom for each turn in the survey, the resulting 1-standard-deviation error is 0.01 in magnitude and 0.7° in phase. The correlation-squared for the second cruise is 0.992 so there is twice as much noise, presumably due to the degraded navigation. However, there are two surveys and roughly twice the degrees of freedom so the resulting errors are the same. There is thus no significance to the difference in γ from one cruise to the next.

Acknowledgments. We thank the members of the Woods Hole SeaSoar group, Jerry Dean, Frank Bahr, and Julie Pallant, for their hard work during all the Subduction cruises. Don Olson of University of Miami provided the satellite SST images to help locate the front. Thanks are extended to Neil Bogue and Mike Hill for participating on the 1992 cruise. The willing assistance of Captain Paul Howland and the crew of the R/V *Oceanus* is appreciated. We gratefully acknowledge the support of the Office of Naval Research under grants N00014-90-J-1496 (D.L.R.), N00014-90-J-1508, and N00014-90-J-1425 (J.R.L.).

References

Bendat, J. S., and A. G. Piersol, *Random Data: Analysis and Measurement Procedures*, 566 pp., John Wiley, New York, 1986.

Bretherton, F. P., R. E. Davis, and C. B. Fandry, A technique for objective analysis and design of oceanographic experiments applied to MODE-73, *Deep Sea Res.*, *23*, 559–582, 1976.

Davis, R. E., Objective mapping by least squares fitting, *J. Geophys. Res.*, *90*, 4773–4777, 1985.

de Szoeke, R. A., On the effects of horizontal variability of wind stress on the dynamics of the ocean mixed layer, *J. Phys. Oceanogr.*, *10*, 1439–1454, 1980.

Flament, P., L. Armi, and L. Washburn, The evolving structure of an upwelling filament, *J. Geophys. Res.*, *90*, 11,765–11,778, 1985.

Hoskins, B. J., and F. P. Bretherton, Atmospheric frontogenesis models: Mathematical formulation and solution, *J. Atmos. Sci.*, *29*, 11–37, 1972.

Iselin, C. O., The influence of vertical and lateral turbulence on the characteristics of waters at mid-depths, *Eos Trans. AGU*, *20*, 414–417, 1939.

Isemer, H.-J., and L. Hasse, *The Bunker Climate Atlas of the North Atlantic Ocean*, vol. 2, *Air-Sea Interactions*, 252 pp., Springer-Verlag, New York, 1987.

Joyce, T. M., On in situ "calibration" of shipboard ADCPs, *J. Atmos. Oceanic Technol.*, *6*, 169–172, 1989.

Le Traon, P.-Y., A method for optimal analysis of fields with spatially variable mean, *J. Geophys. Res.*, *95*, 13,543–13,547, 1990.

Lueck, R. G., Thermal inertia of conductivity cells: Theory, *J. Atmos. Oceanic Technol.*, *7*, 741–755, 1990.

Lueck, R. G., and J. J. Picklo, Thermal inertia of conductivity cells: Observations with a Sea-Bird cell, *J. Atmos. Oceanic Technol.*, *7*, 756–768, 1990.

Luyten, J. R., J. Pedlosky, and H. Stommel, The ventilated thermocline, *J. Phys. Oceanogr.*, *13*, 292–309, 1983.

MacVean, M. K., and J. D. Woods, Redistribution of scalars during upper ocean frontogenesis: A numerical model, *Q. J. R. Meteorol. Soc.*, *106*, 293–311, 1980.

Morison, J., R. Andersen, N. Larson, E. D'Asaro, and T. Boyd, The correction for thermal-lag effects in Sea-Bird CTD data, *J. Atmos. Oceanic Technol.*, *11*, 1151–1164, 1994.

Munk, W., Internal waves and small-scale processes, in *Evolution of Physical Oceanography*, edited by B. A. Warren and C. Wunsch, pp. 264–291, MIT Press, Cambridge, Mass., 1981.

Nurser, A. J. G., and J. C. Marshall, On the relationship between subduction rates and diabatic forcing of the mixed layer, *J. Phys. Oceanogr.*, *21*, 1793–1802, 1991.

Pollard, R., and J. Read, A method for calibrating shipmounted acoustic Doppler profilers and the limitations of gyro compasses, *J. Atmos. Oceanic Technol.*, *6*, 859–865, 1989.

Pollard, R. T., and L. Regier, Large variations in potential vorticity at small spatial scales in the upper ocean, *Nature*, *348*, 227–229, 1990.

Pollard, R. T., and L. A. Regier, Vorticity and vertical circulation at an ocean front, *J. Phys. Oceanogr.*, *22*, 609–625, 1992.

Roden, G. I., On the subtropical frontal zone north of Hawaii during winter, *J. Phys. Oceanogr.*, *10*, 342–362, 1980.

Rudnick, D. L., Intensive surveys of the Azores Front, 2, Inferring the geostrophic and vertical velocity fields, *J. Geophys. Res.*, in press, 1996.

Rudnick, D. L., and R. A. Weller, The heat budget in the North Atlantic subtropical frontal zone, *J. Geophys. Res.*, *98*, 6883–6893, 1993.

Samelson, R. M., Linear instability of a mixed-layer front, *J. Geophys. Res.*, *98*, 10,195–10,204, 1993.

Stommel, H., Determination of water mass properties of water pumped down from the Ekman layer to the geostrophic flow below, *Proc. Natl. Acad. Sci. U.S.A.*, *76*, 3051–3055, 1979.

Veronis, G., On properties of seawater defined by temperature, salinity, and pressure, *J. Mar. Res.*, *30*, 227–255, 1972.

J. R. Luyten, Woods Hole Oceanographic Institution, Woods Hole, MA 02543.

D. L. Rudnick, Scripps Institution of Oceanography, University of California, San Diego, 9500 Gilman Drive, Mail Code 0230, La Jolla, CA 92093. (e-mail: drudnick@ucsd.edu)

(Received April 4, 1995; revised July 27, 1995;
accepted July 28, 1995.)